

The Outer Stellar Halos of Galaxies: how Radial Merger Mass Deposition, Shells and Streams depend on Infall-Orbit Configurations

Geray S. Karademir^{1*}, Rhea-Silvia Remus^{1,2}, Andreas Burkert^{1,3}, Klaus Dolag^{1,4},
Tadziu L. Hoffmann¹, Benjamin P. Moster^{1,4}, Ulrich P. Steinwandel^{1,4}, and
Jielai Zhang^{2,5,6,7}

¹Universitäts-Sternwarte München, Scheinerstraße 1, 81679 München, Germany

²Canadian Institute for Theoretical Astrophysics, 60 St. George Street, University of Toronto, Toronto ON M5S 3H8, Canada

³Max Planck Institute for Extraterrestrial Physics, Giessenbachstr. 1, D-85748 Garching, Germany

⁴Max Planck Institute for Astrophysics, Karl-Schwarzschild-Str. 1, D-85741 Garching, Germany

⁵Department of Astronomy and Astrophysics, University of Toronto, Canada

⁶Dunlap Institute for Astronomy and Astrophysics, Canada

⁷Schmidt Science Fellows in Partnership with the Rhodes Trust

Accepted 2019 April 30. Received 2019 April 30; in original form 2018 August 30

ABSTRACT

Galaxy mergers are a fundamental part of galaxy evolution. To study the resulting mass distributions of different kinds of galaxy mergers, we present a simulation suite of 36 high-resolution isolated merger simulations, exploring a wide range of parameter space in terms of mass ratios ($\mu = 1:5, 1:10, 1:50, 1:100$) and orbital parameters. We find that mini mergers deposit a higher fraction of their mass in the outer halo compared to major mergers, while their contribution to the central mass distribution is highly dependent on the orbital impact parameter: for larger pericentric distances we find that the centre of the host galaxy is almost not contaminated by merger particles. We also find that the median of the resulting radial mass distribution for mini mergers differs significantly from the predictions of simple theoretical tidal-force models. Furthermore, we find that mini mergers can increase the size of the host disc significantly without changing the global shape of the galaxy, if the impact occurs in the disc plane, thus providing a possible explanation for extended low-surface brightness disks reported in observations. Finally, we find clear evidence that streams are a strong indication of nearly circular infall of a satellite (with large angular momentum), whereas the appearance of shells clearly points to (nearly) radial satellite infall.

Key words: galaxies: halos – galaxies: dynamics – galaxies: interactions – galaxies: structure – methods: numerical

1 INTRODUCTION

In the standard cosmological picture, galaxy mergers are a basic and significant process in galaxy evolution. Mergers are important for the hierarchical growth of galaxies, their morphological appearance, their kinematic evolution, and many more aspects (Naab & Ostriker 2017). In our current understanding, the major contributor to stellar mass growth are major mergers ($\mu > 1/4$), while minor ($1/10 < \mu < 1/4$) and mini mergers ($\mu < 1/10$) contribute roughly the same amount of mass to the final galaxy (Rodríguez-Gomez et al.

2016). However, regardless of the mass growth, Hilz et al. (2012) showed that, in the case of spheroidal galaxy merger events, minor mergers lead to an increased size growth and a more rapid surface density profile shape change compared to major mergers. In the case of dry (i.e., gas-poor) minor mergers they leave the inner host structure almost unchanged (Hilz et al. 2013).

This is in agreement with Lagos et al. (2018), who found that dry mergers increase the stellar mass density in the outskirts of the galaxy, while wet mergers tend to build up the bulge of the host galaxy. Using isolated merger simulations, Amorisco (2017) showed that more massive mergers deposit their stars further inside the host galaxy than smaller galax-

* E-mail: karademir@usm.lmu.de

ies, and more concentrated merging satellites can deposit mass further inside than their less compact counterparts of the same mass.

Manifestations of these accretion processes in the form of tidal streams and shells are observed in up to 26% of the galaxies (Atkinson et al. 2013), with massive galaxies with $M > 10^{10.5} M_{\odot}$ being more likely to exhibit tidal features. Similarly, Hood et al. (2018) report a fraction of 17% exhibiting shells or tidal streams from the RESOLVE survey, inspecting more than 1000 galaxies, finding gas-rich galaxies to have a larger likelihood to show signs of tidal interactions than gas-poor galaxies. Martínez-Delgado et al. (2010) also report that several spiral galaxies in the local Universe show significant numbers of giant stellar structures which are remnants of an earlier accretion or interaction process. In case of early-type galaxies alone, Duc (2017) reports a fraction of about 40%. In order to improve the uncertainty of by-eye identification, a fully automated method for identifying and classifying substructures was developed recently by Hendel et al. (2019) (see also Cañas et al. (2019) for a new approach on identifying stellar halos and structures in simulations).

Johnston et al. (2008) already showed that the appearance of shells and streams is a good tracer for the merger history of galaxies, as they strongly depend on accretion time and angular momentum properties of the merger event. Recently, Pop et al. (2018) have shown from hydrodynamical cosmological simulations that shells appear around 18% of their massive galaxies and are usually made through merger events with mass ratios between 1:1 and 1:10 by satellites that merge on low angular momentum orbits. Similarly, Amorisco (2015) showed that shells usually result from more radial merger orbits, while streams are made from merging orbits that are more circular.

The disruption of (smaller) merging galaxies is a plausible mechanism for the origin of diffuse stellar halo light (DSHL) on all scales, i.e., the component of the outer stellar halo that does not show structures like streams and shells anymore¹ (e.g., Zolotov et al. 2009; Cooper et al. 2013, 2015; Longobardi et al. 2018; Hartke et al. 2018). Also, the characteristics of the stellar halo age distribution of the Milky-Way are best reproduced as being formed by the accretion of small satellite galaxies of $\sim 10^{9.5} M_{\odot}$ (Carollo et al. 2018). For galaxy clusters, the DSHL is well studied in the form of the intra-cluster light (e.g., Mihos et al. 2005; Alamo-Martínez & Blakeslee 2017; Montes & Trujillo 2018), and cosmological simulations of galaxy clusters have shown that merger events are the key contributors for the build-up of the diffuse stellar component in these clusters (see Murante et al. 2007, and references therein). For galaxies, the DSHL is dominated by the disruption of satellites with a stellar mass of $\sim 10^{8.5} M_{\odot}$, and its properties are defined by the corresponding merger history (Purcell et al. 2007). It can extend up to a few hundreds of kpc (Zolotov et al. 2009).

This diffuse DSHL (as well as other stellar features in the outskirts of galaxies indicating recent merger events) has recently come back into focus of galaxy research with big surveys for both early-type (e.g., MATLAS (Duc et al. 2015) and VEGAS (Spavone et al. 2017)) and late-type

galaxies (e.g., Dragonfly (Merritt et al. 2016) and GHOSTS (Radburn-Smith et al. 2011; Monachesi et al. 2016)), finding extended stellar halos around most galaxies, although some late-type galaxies have been found to show no or barely any signs of an extended stellar halo component (Merritt et al. 2016; Streich et al. 2016). Using full cosmological simulations, Pillepich et al. (2014) and Remus et al. (2017) showed that the shape of the diffuse outer stellar halo correlates with the accretion history and the total mass of a galaxy, thus providing insight into the details of a galaxy’s formation.

In this work we perform isolated binary merger simulations with extremely high resolution, testing a large parameter space in orbital configurations and mass ratios, to understand the dependence of the mass deposition on these configurations in more detail. As it is already well known from previous work that major merger events completely change the appearance of the galaxies by mixing the stellar (and gaseous) components of both galaxies completely, we do not include these major mergers in our study but instead focus on the impact of minor ($1:4 > \mu > 1:10$) and mini ($\mu < 1:10$) mergers. Especially, we concentrate on understanding the build-up of the stellar halo component without the disruption of an existing disc component in the host, to better understand the large diversity of halos observed around disc galaxies. In Section 2 we describe the merger simulations we perform in detail, and in Section 3 we analyse the dependence of the radial mass deposition of the mergers on the orbital configurations and the merger mass ratio. Finally, in Section 4 we investigate the impact of the merger event on the disc structure of the host and the appearance of shells and streams. We summarize and discuss our results in Section 5.

2 THE SIMULATION SAMPLE

All simulations were carried out using the Tree-SPH code GADGET-3, which is itself descended from the publicly available code GADGET-2 (Springel 2005). We used a state-of-the-art SPH implementation as presented by Beck et al. (2016) to overcome known weaknesses of the SPH formalism that have been pointed out over the last decade (see Agertz et al. 2007 for further details). We used time-dependent artificial viscosity and conduction to enhance the properties of SPH in terms of shock capturing and particle noise reduction in post-shock regions as well as on the surfaces of contact discontinuities.

Moreover, the simulations include complex physics like radiative cooling for optically thin gas which is in ionized equilibrium with a specified background of ultraviolet (UV) radiation (Katz et al. 1996) and star formation (Springel & Hernquist 2003) using a sub-resolution stochastic star-formation approach, where one stellar particle represents a statistical ensemble of stars following the Salpeter (1955) initial mass function (IMF). Supernova feedback from the stars interacts with the interstellar medium (ISM). Also, a supermassive black hole (SMBH) was placed in the center of each galaxy, which can accrete gas with a Bondi-Hoyle accretion model with a hard Eddington limit, and is able to re-emit thermal feedback into its surroundings, as described by Johansson et al. (2009). However, these effects are only

¹ It is possible that these structures are still present but below the detection limits.

Table 1. Main parameters of the created galaxies.

	Mass ratio	v_{200} (km/s)	M_{tot} ($10^{10}M_{\odot}$)	N_{bar}
host	1	160	188.7	4 000 000
satellite	1/5	94	37.7	800 000
	1/10	74	18.9	400 000
	1/50	43	3.8	80 000
	1/100	34	1.9	40 000

of minor importance for the main objective of the current work, which is concerned with the final mass distribution of the remnant.

2.1 Galaxy set-up

The initial conditions for the simulation runs were created using the method described by Springel et al. (2005). We set up the isolated disc galaxies to consist of a dark matter halo, a spherical stellar bulge, and an exponential stellar and gas disc.

The dark matter halo is modeled as a spherical Hernquist profile (Hernquist 1990, 1993), given by

$$\rho_{\text{dm}}(r) = \frac{M_{\text{dm}}}{2\pi} \frac{a}{r(r+a)^3}. \quad (1)$$

Here, M_{dm} is the total dark matter mass of the halo, and a is the scaling parameter. The Hernquist profile is chosen over the NFW profile (Navarro et al. 1997) due to its advantageous analytical properties, in particular that its mass is finite. The scaling parameter a for all our simulations is chosen such that the Hernquist profile in the center matches an NFW profile with a concentration parameter of $c = 12$, using Equation 2 from Springel et al. (2005).

Similarly, the bulge component is also modeled as a Hernquist profile, with a mass fraction of $f_{\text{b}} = 0.01367$ with respect to the total mass of the galaxy.

The stellar disc and the gas disc are set up with an exponential surface density profile given as

$$\Sigma_{\star/\text{gas}} = \frac{M_{\star/\text{gas}}}{2\pi l_{\text{d}}^2} \exp\left(-\frac{r_{\text{polar}}}{l_{\text{d}}}\right), \quad (2)$$

with M_{\star} the stellar mass and M_{gas} the gas mass in the disc, l_{d} a scaling parameter equal for both discs, and r_{polar} the radial component in cylindrical coordinates. The exponential disc contains a gas fraction of $f_{\text{gas}} = 0.2$ and the total mass fraction of both components in the disc is $f_{\text{d}} = 0.041$ with respect to the total mass of the galaxy. The softening-length for the baryonic particles of the simulations is $\epsilon_{\text{bar}} = 0.02$ kpc, while for the dark matter halo $\epsilon_{\text{dm}} = 0.083$ kpc.

The galaxies also contain a black hole in their centers, with a mass fraction of $f_{\text{BH}} = 1.186 \times 10^{-5}$ of the total mass. This results in a mass of $m_{\text{bar}} \sim 1.88 \times 10^4 M_{\odot}$ for each baryonic particle and $m_{\text{dm}} \sim 1.88 \times 10^5 M_{\odot}$ for the dark matter particles, which gives us sufficient mass resolution to study the merger process in great detail.

For this study, five disc galaxies are created using the method described above. Our main galaxy, hereafter referred to as the host galaxy, is a Milky-Way like galaxy with a

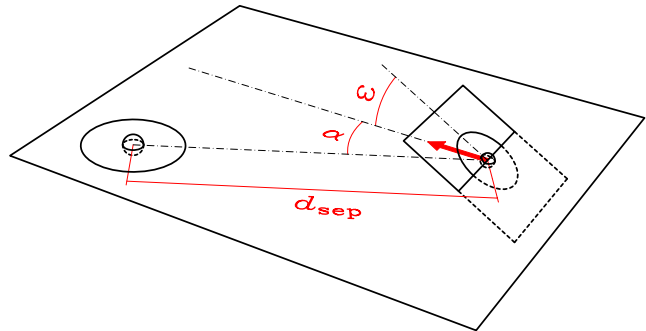


Figure 1. The geometrical set-up for the Family 1 mergers. In this family the satellite approaches the host in the plane of the host disc, with the impact parameter determined by the angle α , while the disc inclination angle of the satellite galaxy is kept fixed at $\omega = 30^\circ$. The initial distance for all mergers is $d_{\text{sep}} = 80$ kpc. The resulting pericentric distances for the different values of α are listed in Table 2.

Table 2. Pericentric distances for the Family 1 mergers.

impact parameter α	10°	20°	30°	40°
pericentric distance (kpc)	1.8	7.0	15.0	24.8

total mass of $M_{\text{tot}} = 1.89 \times 10^{12} M_{\odot}$, corresponding to a virial velocity of $v_{200} = 160$ km/s. The galaxy consists of 10.8 million particles in total, with $N_{\text{dm}} = 6.8 \times 10^6$ dark matter halo particles, $N_{\text{bulge}} = 1 \times 10^6$ bulge stellar particles, $N_{\text{disc}} = 2.4 \times 10^6$ disc stellar particles, and $N_{\text{gas}} = 0.6 \times 10^6$ gas particles.

Because we are interested in seeing how non-spheroidal, two-component galaxies with a disc and a bulge (instead of only simple spheroidal dwarf galaxies) behave in the mergers, we set up the merging galaxies, hereafter referred to as satellite galaxies, as downscaled copies of our host galaxy. Simply downscaling the galaxies is somewhat of an idealization, but it was motivated by the need to provide intrinsically stable satellite galaxies for the simulations. The resulting main parameters of the host galaxy and the four merging satellite galaxies (downscaled in mass by factors of 1/5, 1/10, 1/50, and 1/100 from the host galaxy) are summarized in Table 1.

2.2 Merger set-up

We performed simulations with eight different orbital parameter configurations, where each configuration was performed for four different mass ratios ($\mu = 1:5, 1:10, 1:50, 1:100$), leading to a total of 32 individual galaxy merger simulations. In addition, we performed four simulations with merger mass ratios of $\mu = 1:100$ with special orbital configurations. The resulting 36 simulations cover a broad range of different orbital parameters as well as different mass ratios. As the mass deposition in major mergers has already been studied extensively in previous works, here we focus solely on the contribution of minor mergers ($\mu = 1:5, 1:10$) and mini mergers ($\mu = 1:50, 1:100$).

For the host galaxy, we use the orientation of the disc of this galaxy as the main plane (x - y plane) instead of the orbital plane, and describe the inclination of the orbital plane

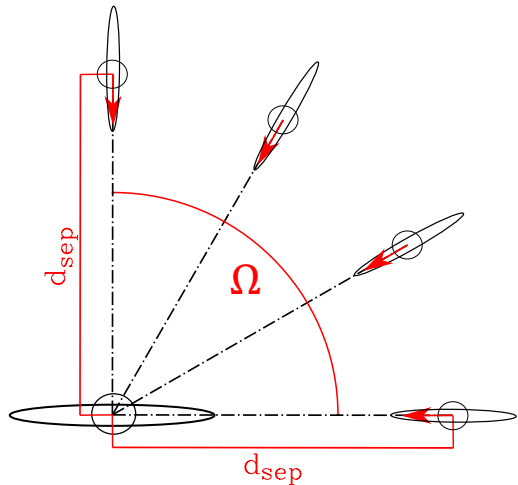


Figure 2. The geometrical set-up for the Family 2 mergers. In this family, the impact parameter is kept fixed at $\alpha = 0^\circ$, while the satellite galaxy approaches the host galaxy from a varying angle Ω above the disc plane of the host galaxy. The initial distance for all mergers is $d_{\text{sep}} = 80$ kpc.

of the merger using the angle Ω as shown in Fig. 2. The impact parameter of the collision is defined by the angle α , which is an equivalent for the pericentric distance, with the corresponding pericentric distances to each value of α used in this study listed in Table 2. These parameters are chosen because they provide freedom in modifying the parameters in every conceivable way, always using the disc plane of the host galaxy as the frame of reference (to better allow studying the impact of the mergers on the host disc).

For all simulations the initial distance between the galaxies is set to $d_{\text{sep}} = 80$ kpc.² The initial approach velocity is equal to the virial velocity regarding the host galaxy, which yields to $v_{\text{vir}} \approx 144.1$ km/s. The velocity vector is initially at an angle α to the geometrical line connecting the two galaxies, as indicated in Fig. 1.

Each simulation is run for approximately 3.5 Gyr after the merger event, which we define at the timestep the discs touch, with two simulation runs extended to 5.5 Gyr after the merger event to study the long term effects.

Our set of simulations can be split into two families. In Family 1, the merger orbits are always in the plane of the host-galaxy disc, i.e., $\Omega = 0^\circ$, while the merging galaxy is tilted by an angle of $\omega = 30^\circ$ relative to this plane³. The impact parameter is varied, $\alpha \in \{10^\circ, 20^\circ, 30^\circ, 40^\circ\}$, which basically means that the orbits change from almost radial to more circular. A sketch of the orbit setup is shown in Fig. 1.

For Family 2, the mergers are always performed on radial orbits, i.e., $\alpha = 0^\circ$, and the disc inclination for the satellite galaxy is fixed at $\omega = 0^\circ$. The orbital angle is varied from edge-on to the host galaxy ($\Omega = 0^\circ$) to face-on ($\Omega = 90^\circ$).

² In our case this is a reasonable distance in a physical sense because it is large enough to keep the initial interaction between the galaxies at a minimum, while at the same time being small enough to avoid wasting computational time on the initial approach.

³ This arbitrary value has been chosen to make the orbit more realistic.

Table 3. Orbital parameters of all mergers.

	α	Ω	ω	Mass ratios	Remarks
Family 1	10°	0°	30°	all	—
	20°	"	"		—
	30°	"	"		—
	40°	"	"		—
Family 2	0°	0°	0°	all	—
	"	30°	"		—
	"	60°	"		—
	"	90°	"		—
Special Cases	0°	10°	0°	only 1:100	—
	10°	10°	"		—
	10°	30°	"		—
	10°	10°	"		retrograde

A sketch of the geometrical setup for Family 2 is shown in Fig. 2.

The four special case simulations are cross-combinations between the systematic variations of Family 1 and Family 2 with the aim to probe the impact of a combination of the impact angle α and the orbital angle Ω , and have been performed only for the $\mu = 1:100$ merger mass ratios since these are the low-cost runs in our simulation set-up. Here we have kept the disc inclination angle of the satellite galaxy for all simulations at $\omega = 0^\circ$. The parameter combinations we have chosen are: $\alpha = 0^\circ$, $\Omega = 10^\circ$; $\alpha = 10^\circ$, $\Omega = 10^\circ$; and $\alpha = 10^\circ$, $\Omega = 30^\circ$. The last simulation in the special case family also has an orbital configuration of $\alpha = 10^\circ$ and $\Omega = 10^\circ$ identical to the second simulation, but in this simulation the disc rotation of the satellite is set up to be retrograde to the disc rotation of the host.

The parameters for all simulations performed in this study are listed in Table 3.

3 RADIAL MASS DEPOSITION

One of the major questions in observations and simulations of stellar halos around galaxies is how to decipher the merger history of a galaxy from only one snapshot in time. For this task, understanding the details of where mass from a disrupted satellite is deposited is of key importance. In order to study the mass deposition of the merger we calculated the corresponding surface density distributions of each remnant approximately 3.5 Gyr after the merger event.

3.1 Orbital and mass-ratio dependence

The radial surface density profiles for all merger simulations from Family 1 and Family 2 at ~ 3.5 Gyr after the merger event are shown in Fig. 3. The first two rows show the results from Family 1, the last two rows show the results from Family 2. In the first and third row, the mergers of different mass ratios at a given impact angle α (first row) or orbital angle Ω (third row) are compared to each other, as indicated in the individual panels. In the second and last row, the mergers of a fixed mass ratio with varying α (second row) and Ω (last row) are compared. Colored solid lines show the resulting surface density profiles for the complete stellar component

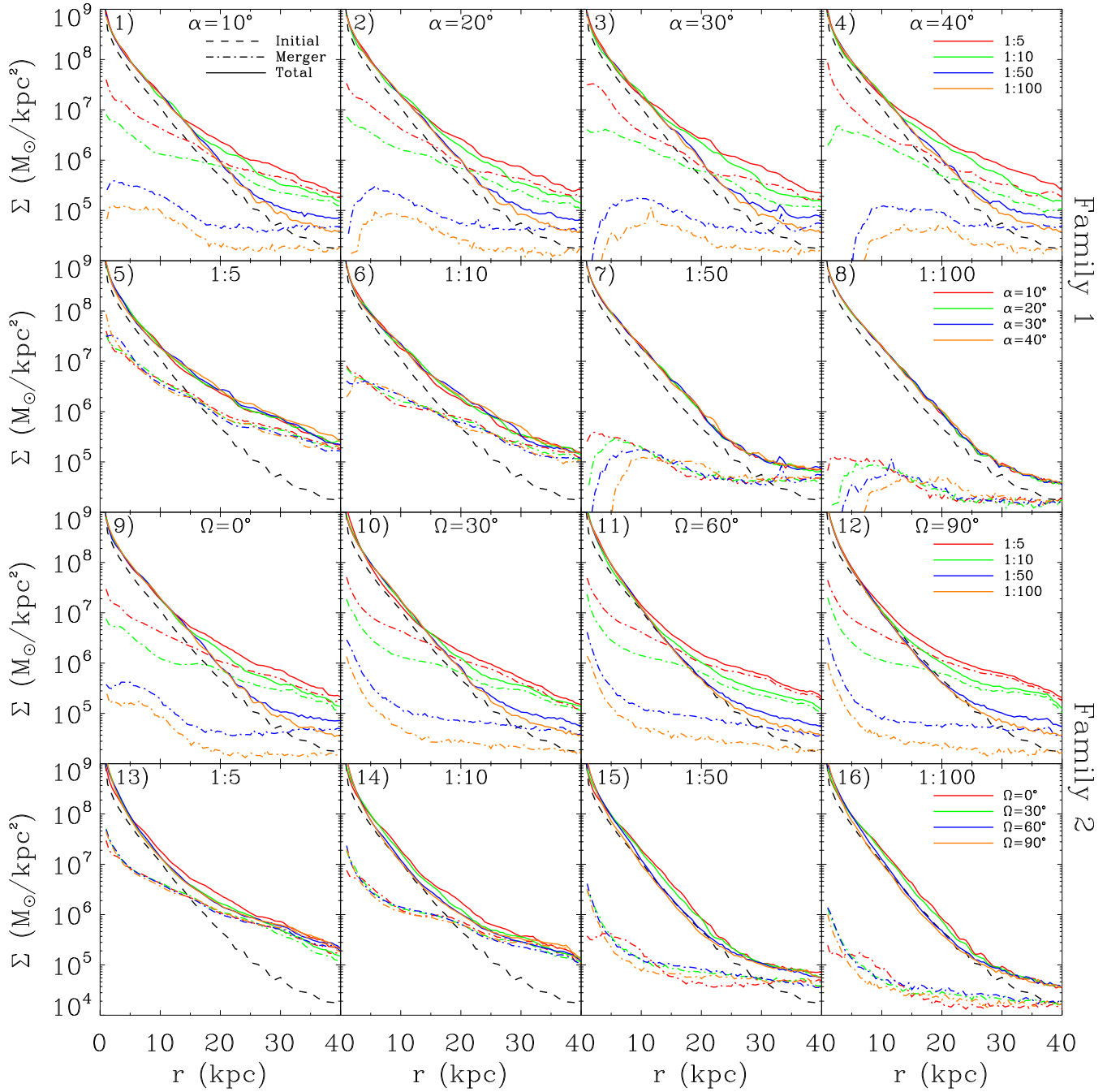


Figure 3. Radial surface density distribution for all simulations at ~ 3.5 Gyr after the beginning of the merging. Solid lines show the total profiles, while dash-dotted profiles mark the radial contribution from the smaller merging galaxy. In all panels, the radial surface density profile of the undisturbed initial main disc galaxy is shown in black. The upper two rows belong to Family 1, the lower two rows to Family 2. The first row compares all mass ratios at a given α , with $\alpha = 10^\circ$, $\alpha = 20^\circ$, $\alpha = 30^\circ$, and $\alpha = 40^\circ$ from left to right, while different colors mark the different mass ratios in each plot of this row. The second row compares results for a fixed mass ratio of 1:5, 1:10, 1:50, and 1:100 from left to right, while different colors mark the different values of α . The third row shows all mass ratios at a fixed Ω , with $\Omega = 0^\circ$, $\Omega = 30^\circ$, $\Omega = 60^\circ$, and $\Omega = 90^\circ$ from left to right, with colors again indicating different mass ratios as for the uppermost row. In the last row results for different Ω at a fixed mass ratio are shown in each panel, with the mass ratios ordered as in the second row and the different colors indicating the different values of Ω used for the mergers.

of the remnant, while the dashed colored lines mark the individual contributions of the satellite galaxies. For reference, the dashed black line in each panel shows the surface density of the isolated, undisturbed host galaxy.⁴

One of the global trends concerning the surface density deposition that can be immediately seen in all panels of Fig. 3 is that, at a certain radius, the contribution from the accreted satellite galaxy starts to dominate the final surface density profile, while the inner part is always dominated by the contribution from the host galaxy. This behavior is independent of the impact angle α or the orbital angle Ω . This crossover point depends mainly on the mass ratio of the merger: a more massive merger has a crossover point closer to the center of the remnant than a less massive merger, where the crossover point lies at larger radii (see panels 1 to 4 and panels 9 to 12 in Fig. 3). The total mass deposited inside the remnant’s disc range depends mainly on the mass ratio: while a 1:100 merger is only able to deposit $\sim 25\%$ of its initial baryonic mass inside the disc range of the remnant, a 1:5 merger can deposit up to 80%. This is in agreement with the results by Amorisco (2017) and confirms earlier studies by Hilz et al. (2013), who showed that minor mergers result in faster size growth, while major mergers result in higher mass growth.

It can also be seen globally that the mini mergers only have a slight impact on the radial surface density distribution of the merger remnant, compared to the initial galaxy. For mini mergers, the surface density profiles of the merger remnant follow the surface density profile of the initial disc galaxy out to large radii of up to ~ 30 kpc ($\sim 4r_{1/2}$), while minor mergers already have a significant influence on the surface density profiles at ~ 15 kpc ($\sim 2r_{1/2}$). For all mergers, the enrichment of the outskirts is much more significant than that of the center of the galaxy.

Starting with Family 1, for the minor mergers (1:5 and 1:10) the surface density distribution is very similar for different impact angles α (panels 5 and 6 of Fig. 3). Mergers of both mass ratios are able to reach the center of the remnant, and therefore significantly disturb the host galaxy.

For the mini mergers (1:50 and 1:100), we find that the impact angle α significantly influences the stellar deposition range of the satellite: for large impact parameters, the satellite cannot contribute to the remnant galaxy’s center anymore (panels 7 and 8 of Fig. 3). Instead, the innermost ~ 5 to 20 kpc ($\sim 1 \dots 3r_{1/2}$) are devoid of any contribution from the satellite galaxy, depending on the mass ratio and impact parameters. The shape of the radial distribution, however, is similar for a given mass ratio, and mainly shifts to the outer regions with increasing α , thereby leaving an increasingly larger region in the center almost vacant.

For Family 2, the mass deposition behaves similar to Family 1 in some aspects. The mass deposition for the minor mergers (panels 13 and 14 of Fig. 3) again only varies slightly for different inclination angles Ω , with no clear systematic trends. Like in Family 1, the center of the host galaxy is always influenced by the merger event.

For the mini mergers, the variation of the inclination angle is much more significant. If $\Omega \geq 30^\circ$, the distribution

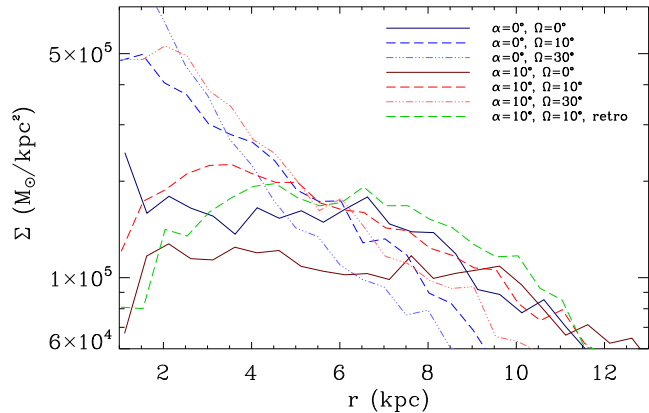


Figure 4. Central surface density distributions of the former satellite particles for seven different $\mu = 1:100$ mergers with orbital configurations as indicated. Here the different effects of the parameters α and Ω can be seen: an increase in α shifts the distribution outwards, while an increase in Ω works in the opposite direction and increases the density in the central region.

varies only marginally (panels 15 and 16 of Fig. 3), but for smaller Ω it shows the same behavior as for Family 1, with the central region becoming devoid of stars from the accreted satellite galaxy. For the mass deposition of a satellite galaxy it is therefore important whether the satellite has to travel through the stellar disc of the host or not.

Since the distribution of the orbital angles of (mini) mergers is not uniform but rather has its highest probability at $\Omega = 0^\circ$ (i.e., along the disc plane of the host; Shao et al. 2018; Welker et al. 2017, 2018), we additionally examine the impact of combinations of small values of α and Ω for our $\mu = 1:100$ mergers. The resulting central radial surface brightness distributions of the former satellite particles of these mini mergers are shown in Fig. 4. For $\alpha = 0^\circ$ and $\Omega \geq 30^\circ$, the density increases steadily inwards. For lower Ω and larger α , the density in the center decreases, and for $\alpha \geq 20^\circ$, $\Omega = 0^\circ$ a region with lower density appears in the center (see the Family-1 mini mergers with $\mu = 1:100$ in panel 8 of Fig. 3). The two parameters α and Ω work opposite to each other. While an increase of Ω increases the density in the central region, a larger α decreases it and shifts the distribution outwards. For the mergers shown in Fig. 4, the fraction of the total satellite mass deposited in the radial range shown (i.e., inside of 13 kpc) varies only slightly between 11...15%, without any distinctive correlation with the orbital parameters.

In addition, one counter-rotating merger simulation was performed (green dashed line in Fig. 4). It can be seen that an inversion of the rotation results in a density distribution shifted outwards but otherwise similar to its co-rotating counterpart (red dashed line). At large radii, however, there are no differences in the mass deposition of the mini mergers, regardless of the orbital configurations. We conclude that the effect of the orbit and impact angles can play an important role for the stellar halos of disc galaxies, as the survival of the disc galaxy can crucially depend on these orbital parameters.

⁴ We let the disc galaxy evolve for the same length as the merger simulations, to account for effects from numerical heating.

3.2 Resulting Sérsic-Indices

As discussed in Section 3.1, mergers can strongly influence the resulting surface density profile shape of the remnant, depending on the mass ratio and impact parameters. In order to give a rough classification of the remnant, we study the light distribution of the remnant (assuming a constant mass-to-light ratio) and calculate the corresponding Sérsic-Index n (Sérsic 1968) parametrizing the radial surface brightness profile

$$\ln(I_R) = \ln(I_0) - kR^{1/n} \quad (3)$$

for each remnant from a face-on surface brightness distribution within a radius of 80 kpc.

We find that for all mergers of both families, the variation of the Sérsic-index due to the merger event follows the same behavior: while the initial galaxy has an index of $n \approx 1.3$ (as expected for an idealized exponential late-type galaxy), it varies after the collision, mainly depending on the different mass ratios. It has to be noted here that newly formed stars (either from the gas in the host or the merger) only make a small contribution. For the $\mu = 1:5$ merger, the remnants show indices of $n \approx 3.5 \dots 6.5$, corresponding to a typical value for an early-type galaxy. The index of the remnant decreases with the mass of the satellite: the 1:10 mergers result in $n \approx 2.2 \dots 4.5$, spanning the whole spectrum of Sérsic indices from late-type to early-type galaxies. It has to be noted that by increasing Ω larger Sérsic indices are reached, while a change in α only results in small changes around $n \approx 2.2$. This clearly shows that minor mergers are fully capable of changing the morphology of a disc galaxy into an S0 or even an early-type galaxy, but for smaller satellites the orbital configuration of the merger is of increasing importance for initiating a morphological change.

For a mass ratio of 1:50, the resulting index reaches $n \approx 1.3 \dots 2.0$, and for the 1:100 mergers we find $n \approx 1.3 \dots 1.4$, almost identical to the index of the initial host galaxy. We conclude that mini mergers are not able to significantly disturb the host disc galaxy; thus, mini mergers appear to be viable candidates for building up stellar halos around disc galaxies.

Interestingly, the orbit for mini mergers plays almost no role in establishing the Sérsic index, while for minor mergers the impact of the orbits on the profile is of much larger importance and the spread in n is much larger. This spread is due to the orbital parameter Ω , with lower Ω causing smaller n . This result can be explained by the larger influence of particle-particle interactions if the satellite is infalling on an orbit in the plane of the host disc.

3.3 Mass distribution by component

For our merger simulations, we used satellite galaxies that were downscaled versions of Milky Way-like disc galaxies, i.e., our satellites have separate stellar disc and bulge components and, due to the initial gas component in the disc, also a component of newly formed stars. Thus, we can investigate the contribution to the mass deposition from the satellite's components at different radii.

As expected, the gas component settles into the central regions of the remnant in all cases. For mini mergers, this is at the position of the innermost peak, which is comprised

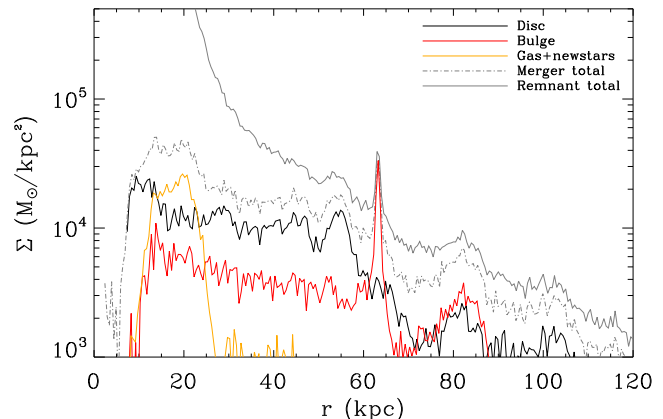


Figure 5. Radial surface density for the Family 1 mini merger ($\mu = 1:100$) with $\alpha = 40^\circ$, split up into the different components of the satellite: the contributions from the disc and bulge components of the accreted satellite are shown as solid black and red lines, respectively. The yellow solid line indicates the contribution of newly formed stars and the gas component of the satellite galaxy, while the full contribution from the accreted component is shown as a dash-dotted gray line. For comparison, the solid gray line shows the total radial surface density profile of the remnant.

largely of gas and newly formed stars in addition to former disc and bulge particles, which can be clearly seen in Fig. 5. This is in agreement with the picture of the gas of the satellite transferring angular momentum to the particles of the host, as a result of which the gas particles can sink down to the central regions of the remnant.

We also find that the contribution of former disc particles to the center of the remnant is higher than that of the bulge particles due to the higher amount of mass contained in the disc compared to the bulge. But especially in the outer regions, basically no bulge particles remain, only disc particles. This is due to the disc stars being the most loosely bound component of the satellite, and therefore large parts of the disc get stripped with high angular momentum. An additional feature which is illustrated in Fig. 5 is the peak in the bulge particle distribution at $r = 64$ kpc. This peak consists of the surviving core of the merger, which is still orbiting the remnant as a bound accumulation of stars, losing mass with every orbit.

3.4 A simple theoretical model

To better understand the characteristics of the distribution of the stripped satellite particles, we compare this with a strongly abstracted theoretical model. We assume a satellite with a Hernquist density profile with initial mass M_S and half-mass radius $r_{1/2}$ that loses its outer, least bound particles as a result of the interaction with the potential of the host galaxy, which we also take to have a Hernquist density profile, with mass M_H and half-mass radius $R_{1/2}$.

We consider two different descriptions for the conditions under which a particle will be stripped from the satellite. The first one (model “A”) is the conventional case of disruption via the tidal forces from the host potential. If we define the satellite radius r_S as the radius that encloses the

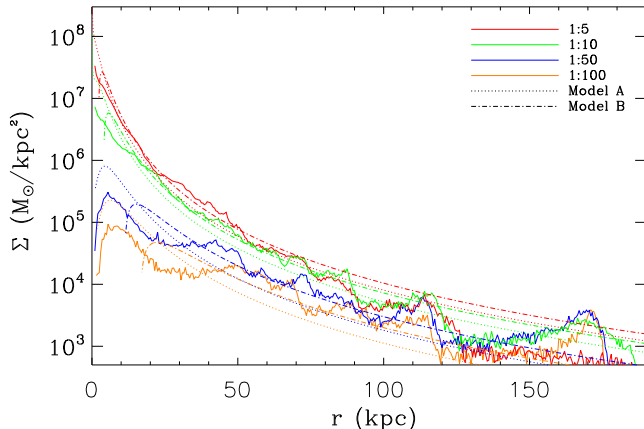


Figure 6. Comparison of the post-merger surface brightness distributions of the former satellite stars for all mass ratios in the Family 1 mergers with $\alpha = 20^\circ$ (solid lines) with those predicted by our simple theoretical models A (dotted lines) and B (dash-dotted lines), scaled to the same merger mass ratios.

remaining mass m , which for a Hernquist profile is

$$r_S(m) = \frac{a}{\sqrt{\frac{M_S}{m} - 1}}, \quad (4)$$

where $a = r_{1/2}/(1 + \sqrt{2})$ is the initial scale radius, then the criterion for stripping the outer particles of the satellite by the tidal forces of the host at distance d from its center is

$$\frac{M_H(d)}{d^2} - \frac{M_H(d + r_S)}{(d + r_S)^2} = \frac{m}{r_S^2}, \quad (5)$$

where $M_H(r) = M_H r^2/(r + a)^2$ is the cumulative mass of the Hernquist-profile host. We divide the satellite into 1000 equal-mass shells, and solve Eq. 5 numerically to obtain the deposition distance d for each mass shell. The simplifying assumption here is that the entire mass shell is deposited where particles at the satellite edge facing the host center become unbound, disregarding internal kinematics of host and satellite, and ignoring any internal rearrangement of the satellite as a result of mass loss.

The basic premise of model A is that the candidate particle and the satellite core are both (apart from their own interaction) acted upon only by the gravitational force of the host galaxy. But this assumption may not be entirely valid: the tighter bound core of the satellite behaves as a joint massive particle inside the host and is thus subject to additional dissipative forces such as dynamical friction, which do not affect a stripped particle. In such a situation the candidate particle will remain with the satellite core only if the binding force between particle and satellite core is stronger than the gravitational force between particle and host galaxy; if not, the particle will become separated from the satellite core and follow an increasingly different trajectory.

To take this consideration into account, in our model B we therefore use the corresponding criterion

$$\frac{M_H(d)}{d^2} = \frac{m}{r_S^2} \quad (6)$$

as the condition for the removal of particles from the satellite at distance d from the host center. Since in this model the satellite core is not assumed to be free-falling with the

particle, the condition for the particle to become unbound will already occur earlier (i.e., farther away from the host). As before, we divide the satellite into 1000 equal-mass shells, and solve Eq. 6 for d to obtain the deposition distance for each mass shell. The same simplifying assumptions are made in model B as in model A (i.e., internal kinematics of host and satellite are disregarded, and internal rearrangement of the satellite as a result of mass loss is ignored).

Despite the crude approximations, both of our simple models display many of the characteristics of the resulting distributions from the simulation. As can be seen in Fig. 6, both models reproduce the global shape of the resulting distribution quite well. Model A in particular reproduces a specific feature of the simulations, namely the decrease of the surface brightness in the central regions for the mini mergers (1:100 and 1:50) in conjunction with the absence of such a decrease for the minor mergers (1:10 and 1:5). However, model A over-predicts the amount of mass in the central regions in all cases; model B shows a better average agreement with the simulations, in particular for the mini mergers, but it under-predicts the central density. As the central regions accumulate a larger fraction of newly formed stars and gas from the satellite, which the simple model is not designed to consider, this latter result may not be entirely unsurprising, and model B appears to offer a better overall description of the distribution of the satellite particles in the remnant.

Two related effects contribute to the differences between the simple theoretical models and the simulation. First, all the mass in the theoretical model satellites is contained in a Hernquist sphere, i.e., the model satellites are much more concentrated than the satellites of the simulations, where only the bulge stars are described by a Hernquist sphere, but not the disc. Therefore, the idealized model satellite would contribute more to the center of the remnant than a less concentrated satellite of the same mass, as shown by Amorisco (2017). Second, the theoretical model assumes that stripping particles from the satellite does not influence the inner regions of the satellite. But this would not be the case for a sphere with an isotropic velocity distribution, since the sphere is only dynamically stable if there is an equilibrium between inward- and outward-moving particles, which, however, will be disturbed by stripping. Thus, the remaining part of the satellite in our theoretical model stays more tightly bound than in a more realistic description.

A different way to quantify the behavior observed in the simulations is to examine the medians of the radial mass distributions found for the satellite galaxy particles in our different merger simulations. With respect to our theoretical models, this median corresponds to the distance from the host at which half of the satellite's particles have been stripped as it moves inwards. This distance can also be expressed via the tidal or Jacobi radius r_J in a two-body system, given by Binney & Tremaine (2008) as

$$r_J \approx \left(\frac{m}{3M}\right)^{1/3} R_0, \quad (7)$$

where m and M are the masses of the orbiting bodies and R_0 their separation. For our purposes, $r_J = r_{1/2}$, $m = M_S/2$, $M = M_H$, and $R_0 = d_{1/2}$, and therefore

$$d_{1/2} = r_{1/2} \left(\frac{6M_H}{M_S}\right)^{1/3}. \quad (8)$$

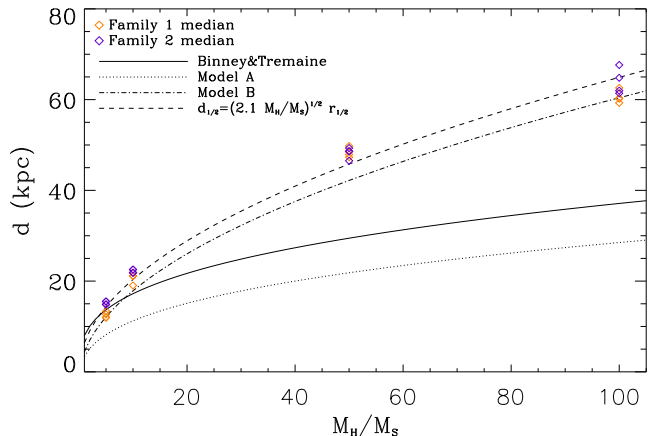


Figure 7. The median of the radial mass distribution of the former satellite stellar particles for all Family 1 (orange diamonds) and Family 2 (violet diamonds) mergers, compared to the corresponding medians predicted by idealized theoretical models.

In Figure 7 we plot the medians of the radial mass distributions of the satellite particles from the simulations, compared to this analytical approximation and the corresponding results from our simple theoretical models A and B.

The curve resulting from our model A (dotted line) has a shape very similar to that of the analytic curve using the Jacobi radius (solid line). Both of these describe the stripping purely as a result of tidal forces, our model A assuming a satellite in free fall towards the host, the analytic description assuming a satellite on a circular orbit. In our Eq. 5, however, d is the distance between the host center and the leading edge of the satellite, whereas in Eq. 8 it refers to the distance between host center and satellite center, and thus our model A curve lies at least one half-mass radius further inwards than the analytic curve. Furthermore, our model assumes the host to be a Hernquist sphere, which has a shallower potential gradient (and thus allows the satellite to penetrate further into the host before being stripped) than the point-mass assumed for the host in the analytic description.

The curve resulting from our model B (dash-dotted line)

$$d_{1/2} = r_{1/2} \left(\sqrt{\frac{2M_H}{M_S}} - \frac{R_{1/2}/r_{1/2}}{1 + \sqrt{2}} \right) \quad (9)$$

(plotted for $R_{1/2}/r_{1/2} = 1$) shows a much better match to the actual medians from the simulations, for which we have sketched a rough fit as the dashed line. This result indicates that a description based solely on tidal forces does not capture all essential aspects of an actually occurring merger. Of course, one aspect that our simple model cannot describe is the tendency of a disturbed system to continuously re-virialize, leading to an expansion of the infalling satellite simultaneously to the stripping process. This would lead to a larger characteristic radius, lower densities, and an easier stripping of the remaining mass, overall resulting in mass being deposited at larger radii. This effect has been recently described by van den Bosch et al. (2018) for dark-matter-only halos, and is likely to occur for galaxies as well.

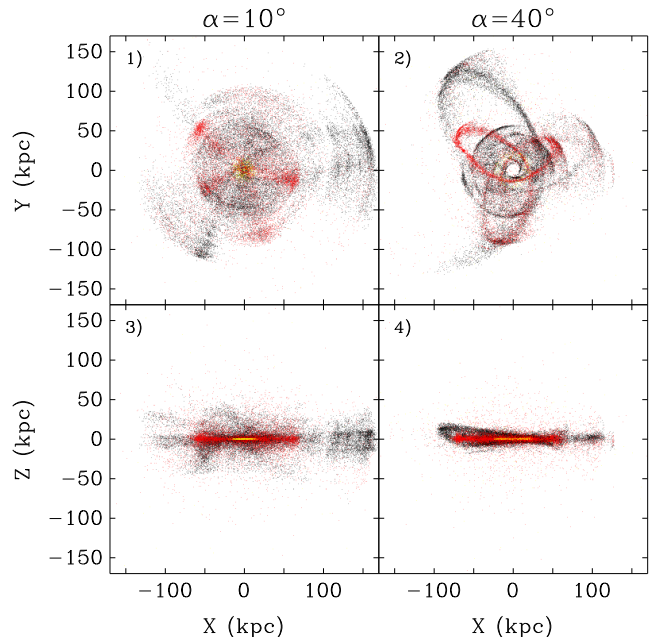


Figure 8. Shells and streams for two examples of $\mu = 1:100$ mergers at $t = 5.5$ Gyr after the merger event. For the simulations, all parameters are identical but the impact angle α , with $\alpha = 10^\circ$ for the example in the left panels and $\alpha = 40^\circ$ for the example in the right panels. Only the stars from the satellite galaxy are shown here, with disc stars in black, bulge stars in red, and newly formed stars in yellow.

4 SHELLS, STREAMS, AND DISK GROWTH

As shown in Section 3, the host disc galaxy loses its initial form and becomes more and more isotropic for minor mergers in general and for larger satellite masses in particular. However, we find that the appearance of shell or stream structures does not depend, in general, on the merger mass ratio but is closely correlated with the impact angle α : for small α values up to $\alpha \sim 10^\circ$, all mergers produce shells but no streams, while for larger values of α only streams appear, and no shells at all. Figure 8 illustrates this behavior: the left panels show the face-on (upper panel) and edge-on (lower panel) projections of the mass distribution of a $\mu = 1:100$ satellite galaxy merger with $\alpha = 10^\circ$, $\Omega = 0^\circ$ and $\omega = 30^\circ$, while the right panels show the same for the identical merger scenario but $\alpha = 40^\circ$. As can be seen very clearly, the merger with the small impact angle produces only shell structures, while the merger with the large impact angle causes streams but no shells. This is in good agreement with the results from Amorisco (2015) who also reported that shells are made by mergers on radial orbits, while streams appear for more circular orbits. This behavior can be seen in more detail in Figs. A3 and A4 in Appendix A, where the same diagrams as in Fig. 8 are shown for the full sample of simulations from Family 1.

We also find that there is no effect of the orbital angle Ω on the appearance of shells or streams, although all structures are slightly less pronounced for the face-on ($\Omega = 90^\circ$) collisions (see Figs. A5 and A6). To summarize, we find clear evidence that galaxy shells only occur for central (radial) hits, and are more prominent for orbits along the major axis of the host and less pronounced for face-on mergers. By vi-

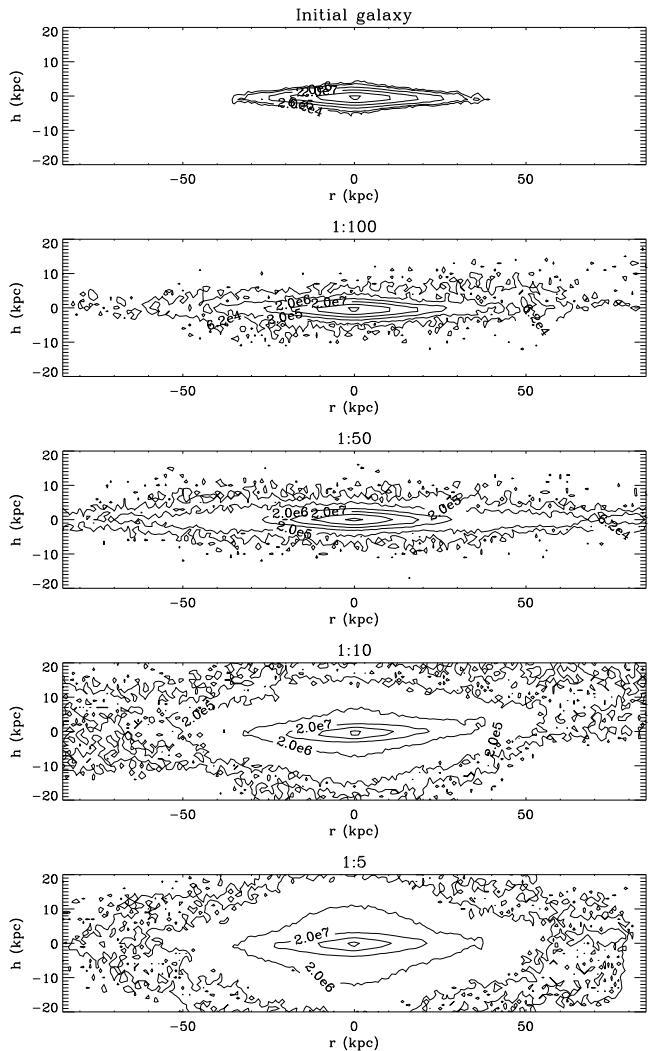


Figure 9. The resulting edge-on density distribution of the remnant after a relaxation time of ~ 3.5 Gyr for the Family 2 mergers with $\Omega = 0^\circ$ and $\alpha = 0^\circ$. For comparison, the uppermost panel shows the undisturbed disc evolved for the same time as the merger simulation. The other panels show, from top to bottom, the results for the $\mu = 1:100$, $1:50$, $1:10$, and $1:5$ merger mass ratio simulations. The contour lines are in units of M_\odot/kpc^2 .

sual inspection of the formation of streams and shells in the simulations, we find that the lifetime of streams appears to be longer than that of shells. The latter seem to be more rapidly smoothed out into a continuous distribution, as it can be seen in Fig. 8.

Under certain conditions it is possible that the mergers mainly increase the host disc size without puffing up the disc. Figure 9 shows the edge-on view of the host disc for the Family 2 mergers with $\Omega = 0^\circ$ and $\alpha = 0^\circ$, with $\mu = 1:5$, $1:10$, $1:50$, and $1:100$ from bottom to top. The uppermost panel shows the undisturbed disc galaxy evolved for $t = 3.5$ Gyr. As can be clearly seen, the disc of the galaxy grows up to two times its original size by a $\mu = 1:100$ merger, and even more for the $\mu = 1:50$ merger. Meanwhile, the disc-height remains constant with a scale-height of $h \approx 1.5$ kpc for both mini mergers. With increasing mass of the merging

satellite, the size of the disc does not increase any further, but instead the disc height starts to grow significantly while the disc structure is destroyed. In the lower panels of Fig. 9 this effect can be seen very prominently.

Besides the mass ratio, the orbital parameters are also very important in forming such large discs. An increase in disc size can only be seen for $\Omega < 30^\circ$. If the inclination of the merger rises to $\Omega \geq 30^\circ$, the density distribution becomes much more spherical.

The observation of such a giant, low-surface-brightness stellar disc around NGC 2841 has just recently been reported by Zhang et al. (2018). The observed disc has a radial extent of ~ 70 kpc with a mass surface density at the edge of $\sim 0.1 M_\odot/\text{pc}^2$ which is similar to the outermost contour lines in Fig. 9. Nevertheless, as we are assuming a constant mass-to-light ratio, a proper comparison would require mimicking the observations (e.g. computing the corresponding fluxes in the corresponding band and applying surface brightness cuts). This suggests mini mergers as a possible explanation for the origin of this extended disc, in particular also because NGC 2841 at the same time does not show signs of a spherical stellar halo. It is quite possible that more than one mini merger would be needed to build up the extended disc to the observed surface brightness; however, as there are now several observational reports of satellite galaxies being aligned in planes around their host galaxies (e.g., Tully et al. 2015; Müller et al. 2016; Fritz et al. 2018), multiple mini mergers building up such a disc would indeed appear possible, although we cannot yet comment on the probability of this happening.

5 SUMMARY AND CONCLUSION

Mergers play an essential role in a galaxy’s evolution, shaping both its morphology and driving its mass growth. Numerical simulations of mergers have become a key tool in understanding the diversity of observed galactic structures and their environments. Cosmological simulations, having now reached resolution levels making it possible to resolve individual galaxies even in huge simulation volumes with box lengths of a gigaparsec or more, have proved important in explaining the statistical properties of galaxy populations. For understanding the details of merger processes, however, individually set up high-resolution merger simulations with carefully controlled configurations are still indispensable.

We performed 36 simulations of isolated mergers between two disc galaxies with mass ratios varying between $\mu = 1:5$ and $1:100$ with high particle resolution. With these simulations, we provide a systematic study of the influence of different orbit configurations on the mass distribution of the final merger remnant and specifically the mass distribution of the disrupted satellite galaxy within the final merger remnant.

We find that mergers with mass ratios from $\mu = 1:10$ to $1:5$, so-called minor mergers, already have a sufficient impact to significantly alter the morphological appearance of the host galaxy, as measured by the Sérsic-index. Mergers with smaller satellites (mini mergers), however, barely change the Sérsic-index of the host, leading primarily to an increase of the disc size and a slight puffing-up of the disc, depending on the infall direction of the satellite relative to the host disc.

Perhaps the most important result is that especially the mini mergers deposit their mass at much larger radii than expected from assuming that the breakup of the satellite results purely from the tidal forces of the host galaxy – the medians of the radial post-merger distribution of the former satellite stars in the simulations are larger by up to a factor of 2 in radius than predicted by this model. However, if we do not assume that the satellite core is free-falling with the stripped particles (because it will be subject to additional forces such as dynamical friction that do not affect the stripped particles) and instead consider only the actual binding forces, then the predicted medians agree much better with those from the simulations. This indicates that a description based solely on tidal forces does not capture all essential aspects of actual mergers.

While minor mergers always deposit part of their mass to the center of the host independent of the orbital parameters, mini mergers cannot reach the center if they approach the host on circular orbits close to the disc plane of the host. In fact, mini mergers can contribute to building up a stellar halo around the host without significantly disturbing the center, depositing most of their mass in the outskirts. If the satellite approaches in the disc plane, this halo can even be disc-like in shape, thus offering a possible explanation for the observed existence of such extended halo-less discs (Zhang et al. 2018).

Interestingly, the impact parameter angle α and the orbital plane angle Ω have opposing effects on the radial mass distribution of the satellite particles within the remnant, while an inversion of the internal rotation of the merger only has a minor effect. Increasing α leads to a decrease of the satellite contribution to the center of the merger remnant, while increasing Ω causes more satellite particles to be deposited at the center. Furthermore, α plays a crucial role for the emergence of shell and stream features: streams appear for $\alpha \geq 30^\circ$ (pericentric distance ≥ 15 kpc), and values of $\alpha \leq 10^\circ$ (pericentric distance ≤ 1.8 kpc) lead to distinct shell structures, independent of the choice of Ω . Intermediate values of α lead to structures showing features of both streams and shells. To conclude, streams are a strong indication of nearly circular infall of a satellite (with a large angular momentum), whereas the appearance of shells clearly points to (nearly) radial satellite infall.

ACKNOWLEDGEMENTS

We would like to thank the reviewer for his/her insightful comments and constructive remarks. The Simulations were run at the Leibniz Computing Center, Germany, as part of the project pr86re. UPS and BPM acknowledge an Emmy Noether grant funded by the Deutsche Forschungsgemeinschaft (DFG, German Research Foundation) with the project number MO 2979/1-1.

REFERENCES

Agertz, O., Moore, B., Stadel, J., et al. 2007, *MNRAS*, 380, 963
 Alamo-Martínez, K. A. & Blakeslee, J. P. 2017, *ApJ*, 849, 6
 Amorisco, N. C. 2015, *MNRAS*, 450, 575
 Amorisco, N. C. 2017, *MNRAS*, 464, 2882
 Atkinson, A. M., Abraham, R. G., & Ferguson, A. M. N. 2013, *ApJ*, 765, 28

Beck, A. M., Murante, G., Arth, A., et al. 2016, *MNRAS*, 455, 2110
 Binney, J. & Tremaine, S. 2008, *Galactic Dynamics: Second Edition* (Princeton University Press)
 Cañas, R., Elahi, P. J., Welker, C., et al. 2019, *MNRAS*, 482, 2039
 Carollo, D., Tissera, P. B., Beers, T. C., et al. 2018, *ApJ*, 859, L7
 Cooper, A. P., D'Souza, R., Kauffmann, G., et al. 2013, *MNRAS*, 434, 3348
 Cooper, A. P., Parry, O. H., Lowing, B., Cole, S., & Frenk, C. 2015, *MNRAS*, 454, 3185
 Duc, P.-A. 2017, in *IAU Symposium*, Vol. 321, *Formation and Evolution of Galaxy Outskirts*, ed. A. Gil de Paz, J. H. Knapen, & J. C. Lee, 180–182
 Duc, P.-A., Cuillandre, J.-C., Karabal, E., et al. 2015, *MNRAS*, 446, 120
 Fritz, T. K., Battaglia, G., Pawlowski, M. S., et al. 2018, *A&A*, 619, A103
 Hartke, J., Arnaboldi, M., Gerhard, O., et al. 2018, *A&A*, 616, A123
 Hendel, D., Johnston, K. V., Patra, R. K., & Sen, B. 2019, *MNRAS*, 1047
 Hernquist, L. 1990, *ApJ*, 356, 359
 Hernquist, L. 1993, *ApJS*, 86, 389
 Hilz, M., Naab, T., & Ostriker, J. P. 2013, *MNRAS*, 429, 2924
 Hilz, M., Naab, T., Ostriker, J. P., et al. 2012, *MNRAS*, 425, 3119
 Hood, C. E., Kannappan, S. J., Stark, D. V., et al. 2018, *ApJ*, 857, 144
 Johansson, P. H., Naab, T., & Burkert, A. 2009, *ApJ*, 690, 802
 Johnston, K. V., Bullock, J. S., Sharma, S., et al. 2008, *ApJ*, 689, 936
 Katz, N., Weinberg, D. H., & Hernquist, L. 1996, *ApJS*, 105, 19
 Lagos, C. d. P., Stevens, A. R. H., Bower, R. G., et al. 2018, *MNRAS*, 473, 4956
 Longobardi, A., Arnaboldi, M., Gerhard, O., Pulsoni, C., & Söldner-Rembold, I. 2018, *A&A*, 620, A111
 Martínez-Delgado, D., Gabany, R. J., Crawford, K., et al. 2010, *AJ*, 140, 962
 Merritt, A., van Dokkum, P., Abraham, R., & Zhang, J. 2016, *ApJ*, 830
 Mihos, J. C., Harding, P., Feldmeier, J., & Morrison, H. 2005, *ApJL*, 631, L41
 Monachesi, A., Bell, E. F., Radburn-Smith, D. J., et al. 2016, *MNRAS*, 457, 1419
 Montes, M. & Trujillo, I. 2018, *MNRAS*, 474, 917
 Müller, O., Jerjen, H., Pawlowski, M. S., & Binggeli, B. 2016, *A&A*, 595, A119
 Murante, G., Giovalli, M., Gerhard, O., et al. 2007, *MNRAS*, 377, 2
 Naab, T. & Ostriker, J. P. 2017, *Annual Review of Astronomy and Astrophysics*, 55, 59
 Navarro, J. F., Frenk, C. S., & White, S. D. M. 1997, *ApJ*, 490, 493
 Pillepich, A., Vogelsberger, M., Deason, A., et al. 2014, *MNRAS*, 444, 237
 Pop, A.-R., Pillepich, A., Amorisco, N. C., & Hernquist, L. 2018, *MNRAS*, 480, 1715
 Purcell, C. W., Bullock, J. S., & Zentner, A. R. 2007, *ApJ*, 666, 20
 Radburn-Smith, D. J., de Jong, R. S., Seth, A. C., et al. 2011, *ApJS*, 195, 18
 Remus, R.-S., Burkert, A., & Dolag, K. 2017, in *IAU Symposium*, Vol. 321, *Formation and Evolution of Galaxy Outskirts*, ed. A. Gil de Paz, J. H. Knapen, & J. C. Lee, 84–86
 Rodríguez-Gomez, V., Pillepich, A., Sales, L. V., et al. 2016, *MNRAS*, 458, 2371
 Salpeter, E. E. 1955, *ApJ*, 121, 161
 Sérsic, J. L. 1968, *Atlas de Galaxias Australes*

- Shao, S., Cautun, M., Frenk, C. S., et al. 2018, *MNRAS*, 476, 1796
- Spavone, M., Capaccioli, M., Napolitano, N. R., et al. 2017, *A&A*, 603, A38
- Springel, V. 2005, *MNRAS*, 364, 1105
- Springel, V., Di Matteo, T., & Hernquist, L. 2005, *MNRAS*, 361, 776
- Springel, V. & Hernquist, L. 2003, *MNRAS*, 339, 289
- Streich, D., de Jong, R. S., Bailin, J., et al. 2016, *A&A*, 585, A97
- Tully, R. B., Libeskind, N. I., Karachentsev, I. D., et al. 2015, *ApJL*, 802, L25
- van den Bosch, F. C., Ogiya, G., Hahn, O., & Burkert, A. 2018, *MNRAS*, 474, 3043
- Welker, C., Dubois, Y., Pichon, C., Devriendt, J., & Chisari, N. E. 2018, *A&A*, 613, A4
- Welker, C., Power, C., Pichon, C., et al. 2017, *ArXiv e-prints*, arXiv:1712.07818
- Zhang, J., Abraham, R., van Dokkum, P., Merritt, A., & Janssens, S. 2018, *ApJ*, 855, 78
- Zolotov, A., Willman, B., Brooks, A. M., et al. 2009, *ApJ*, 702, 1058

APPENDIX A: SHELLS AND STREAMS FOR ALL MERGERS

We show the stellar particle distributions of the satellite galaxy at a time $t \sim 3.5$ Gyr after the merger event (i.e., 4.2 Gyr after the beginning of the simulation, with the merger event taking place approximately 0.7 Gyr after the simulation begins, this value varying slightly with the impact angle α). All distributions are shown in both edge-on (X - Z) and face-on (X - Y) views, referring to the orientation of the host galaxy (which, however, is not shown in these plots). In all figures, colors show the stars from the different components of the initial satellite galaxies: black—disc stars; red—bulge stars; yellow—gas and newly formed stars, as in Fig 8.

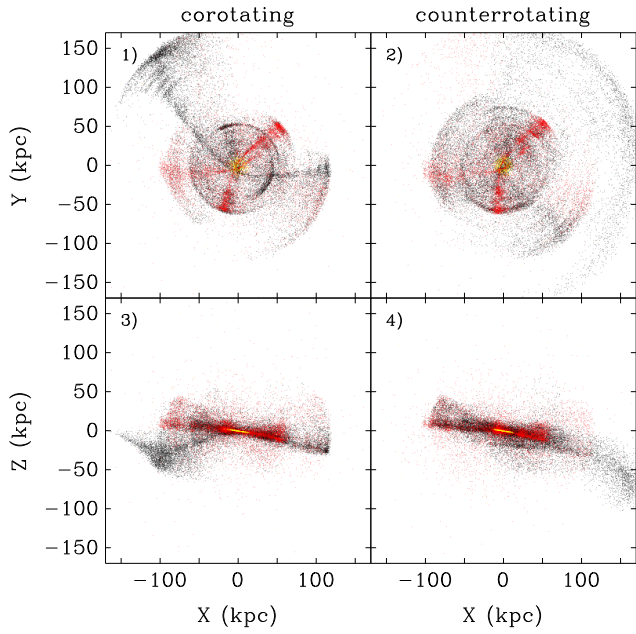


Figure A1. Face-on (top panels) and edge-on (bottom panels) views of the distribution of the satellite particles for the special case simulations with $\alpha = 10^\circ$ and $\Omega = 10^\circ$, where the discs are corotating (left panels) and counterrotating (right panels).

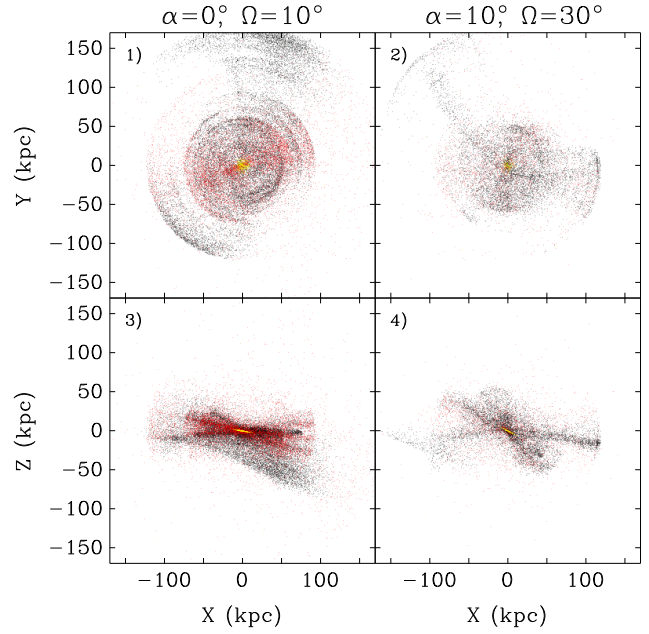


Figure A2. Face-on (top panels) and edge-on (bottom panels) views of the distribution of the satellite particles for the special case simulations with $\alpha = 0^\circ, \Omega = 10^\circ$ (left panels), and $\alpha = 10^\circ, \Omega = 30^\circ$ (right panels).

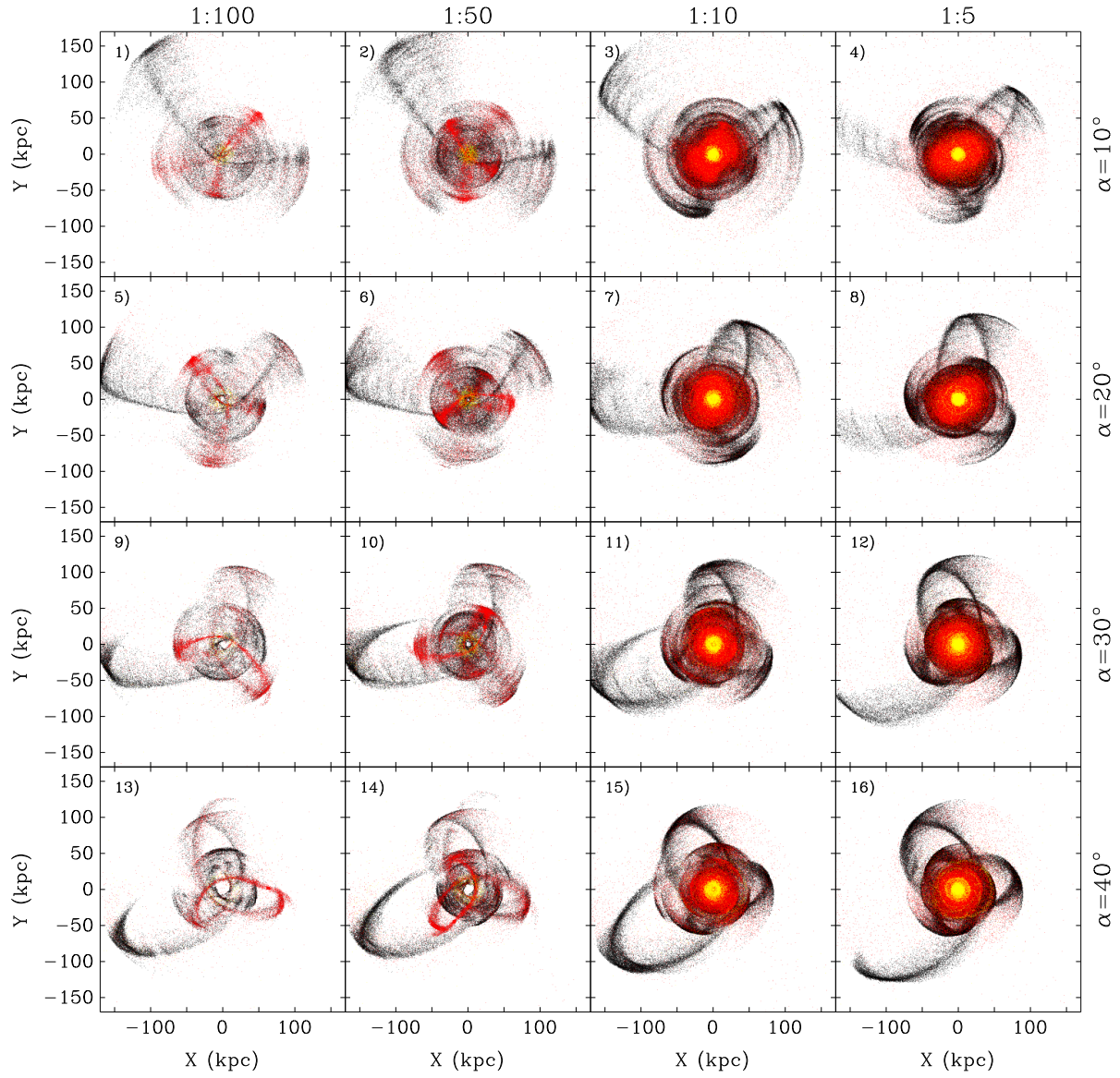


Figure A3. Face-on view of all satellite particles for all Family 1 mergers.

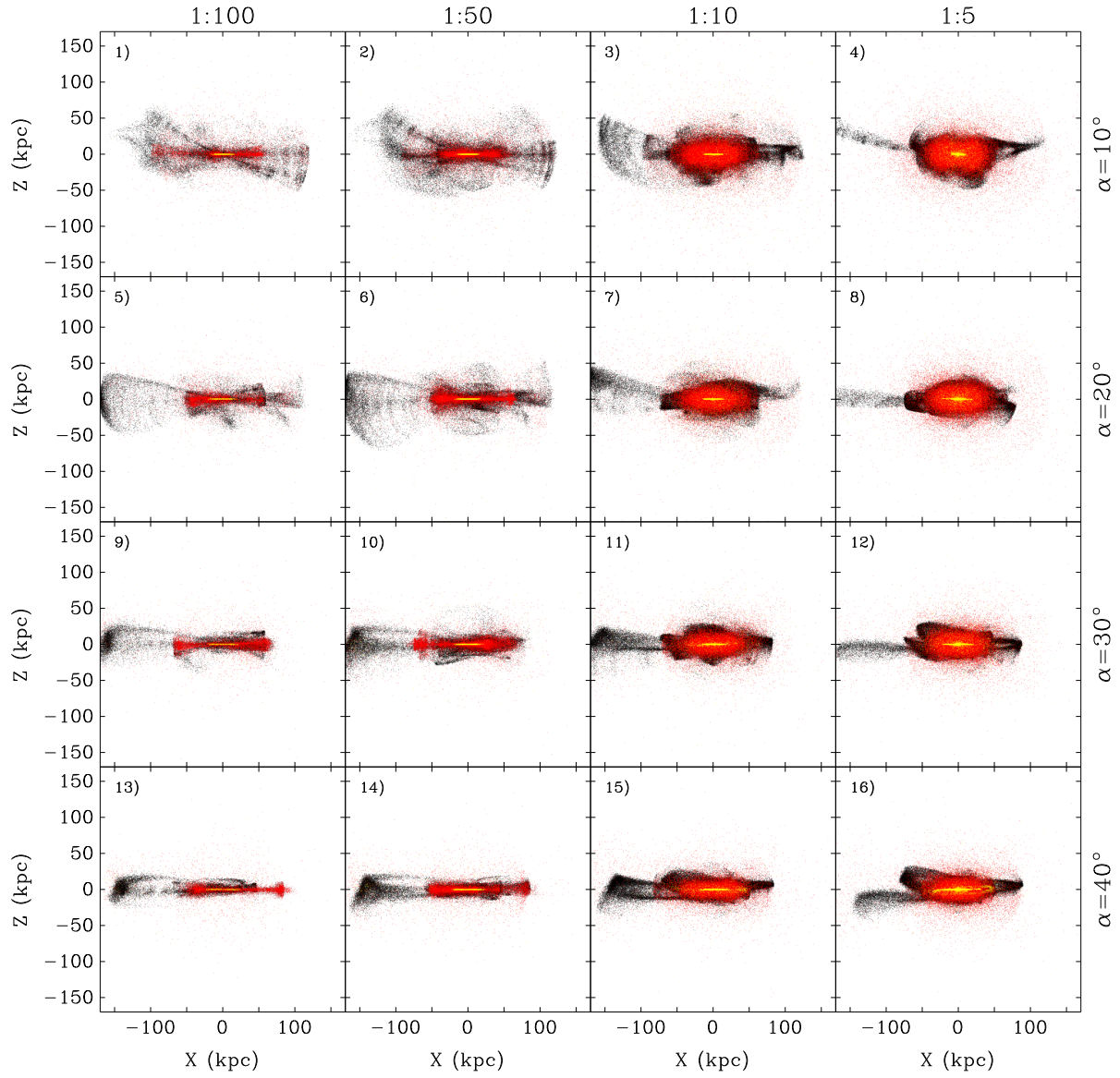


Figure A4. Edge-on view of all satellite particles for all Family 1 mergers.

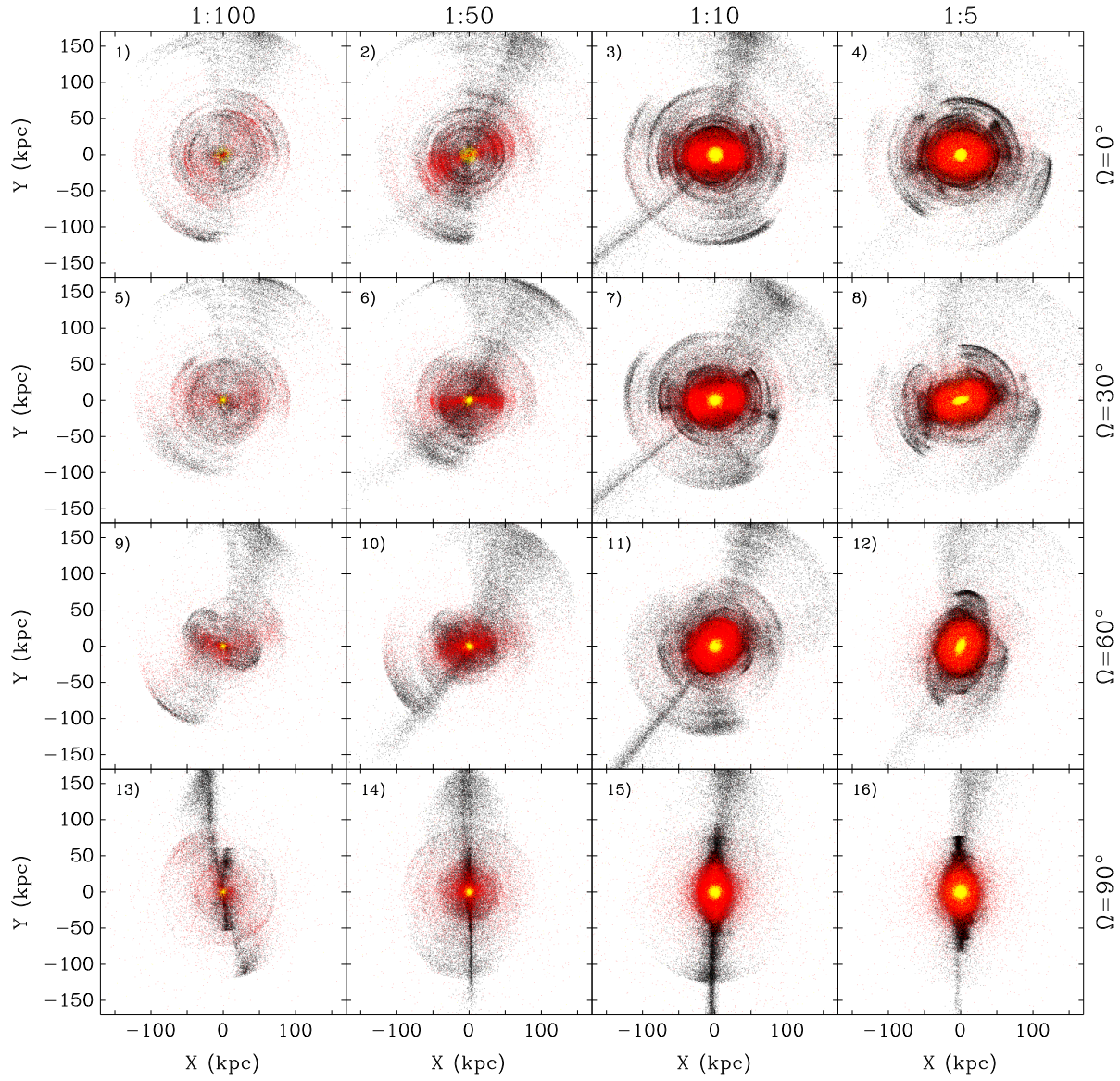


Figure A5. Face-on view of all satellite particles for all Family 2 mergers.

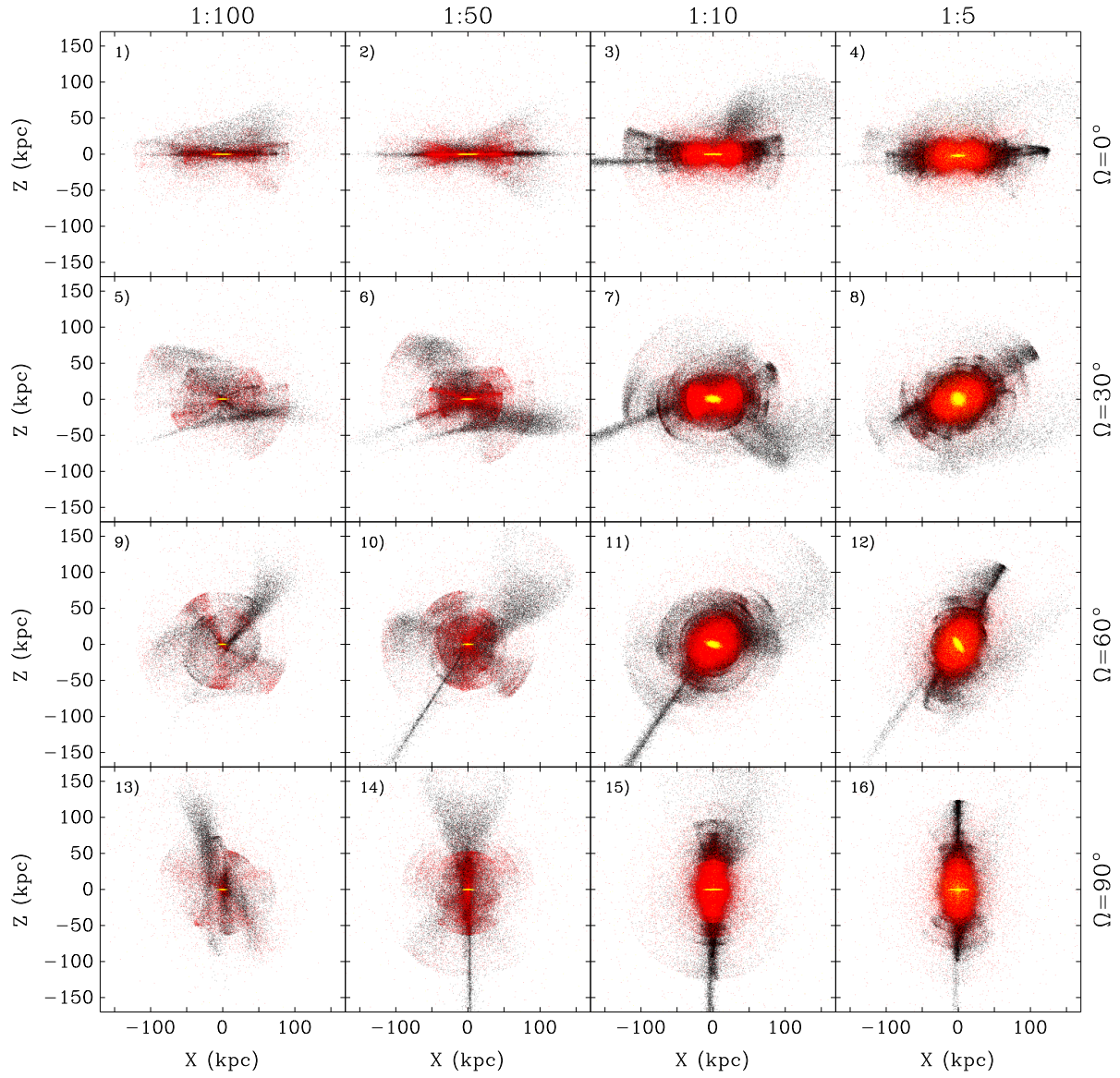


Figure A6. Edge-on view of all satellite particles for all Family 2 mergers.